J Mol Model (2009) 15:1291–1297
DOI 10.1007/s00894-009-0488-z

ORIGINAL PAPER

# Parameterization of aromatic azido groups: application as photoaffinity probes in molecular dynamics studies

**Gilles Pieffet · Pavel A. Petukhov**

Received: 1 December 2008 / Accepted: 6 February 2009 / Published online: 14 March 2009


**Abstract** The accuracy of molecular dynamics (MD) simulations is limited by the availability of parameters for the molecular system of interest. In most force fields, parameters of common chemical groups are already present. With the development of novel small organic molecules as probes to study biological systems, more chemical groups require parameterization. An azide group is often used in studies of biological systems but computational studies are still impeded by the lack of parameters. In this paper, we present a set of molecular mechanics (MM) parameters for aromatic and aliphatic azido groups, and their application in MD simulations of a photoaffinity probe currently used in our laboratory for mapping binding modes available in the active site of histone deacetylases. The parameters were developed for the generalized Amber force field (GAFF) using density functional theory (DFT) calculations at B3LYP 6-311G(d) level. The parameters were validated by geometry optimization and MD simulations.

**Keywords** Force field · Parameterization · Azido groups · Molecular dynamics · Molecular mechanics · Photoaffinity probes

**Electronic supplementary material** The online version of this article (doi:10.1007/s00894-009-0488-z) contains supplementary material, which is available to authorized users.

G. Pieffet · P. A. Petukhov (✉)
Department of Medicinal Chemistry and Pharmacognosy,
College of Pharmacy, University of Illinois at Chicago,
833 South Wood Street,
Chicago, IL 60612, USA
e-mail: pap4@uic.edu

## Introduction

Molecular dynamic (MD) simulations are the method of choice to study small and macromolecular systems as they provide valuable information on their dynamic behavior at the atomic level. Combining molecular mechanics (MM) force field parameters for macro- and small molecules in MM/MD calculations is usually a challenging task as historically MM force fields were designed for either one of these two systems. Until recently, simulating the interactions between small chemical compounds and proteins, a typical task in studying drug–receptor interactions, meant having to re-parameterize the original force field parameters developed for small organic compounds for the force field used with the protein. To address this issue a general Amber force field (GAFF) for common chemical groups was designed to be compatible with the popular series of Amber force field for proteins and nucleic acids, which significantly accelerated the setup of ligand–protein systems for MM/MD calculations. The number of chemical groups parameterized for GAFF is gradually increasing since more and more small molecule ligands bound to their macromolecular targets require MM/MD simulations. We recently developed a series of photolabeling ligands containing $N_3$-aryl ($N_3$-Ar) and $N_3$-alkyl ($N_3$-Alk) groups to probe the binding site of histone deacetylases (HDAC) [1], a family of enzymes that are targeted in the design of therapeutics for cancer and neurological diseases [2–7]. Although the Amber parameters for an $N_3$-Alk group have been previously reported as a part of the parameterization of zidovudine (AZT) [8], there are no parameters for an $N_3$-Ar group, which are required to model Photoaffinity Probe **1** (Fig. 1), which is currently used in our laboratory [1].

In this study we have determined a set of MM parameters for the $N_3$-Ar group and validated them using

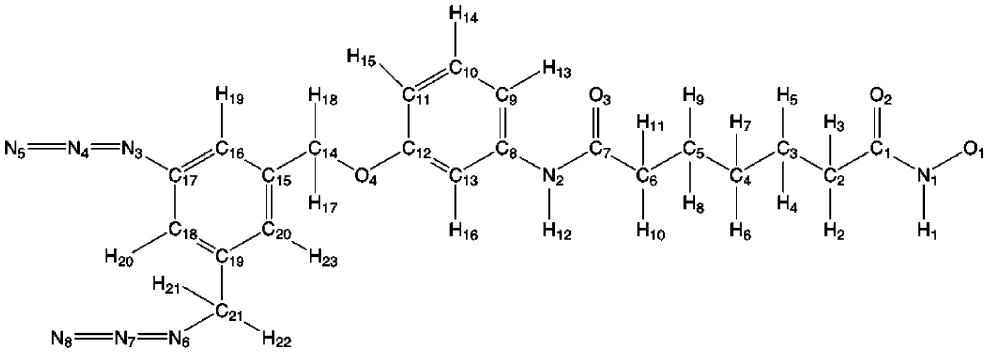

**Fig. 1** Schematic illustration of deprotonated photoaffinity Probe **1**

simulations with Compound **1**. For consistency with the new aromatic $N_3$-Ar parameters, we also re-calculated parameters for the aliphatic $N_3$-Alk group.

## Materials and methods

High transferability of the MM parameters in GAFF is achieved by describing the most common chemical groups using a limited set of atom types that are devised to be as general as possible, and an energy function (Eq. 1) that does not include cross-terms to describe the molecular system [9, 10]. The MM parameters were calculated by fitting the quantum mechanical (QM) potential energy surface (PES) using standard procedures. The regression parameters correspond to the force constants $K_r$ and $K_\theta$ of the bonds and angles PES, respectively, and to the height of the potential $V_n$ in the case of the dihedrals PES (Table 1).

$$E = \sum_{bonds} K_r(r - r_0)^2 + \sum_{angles} K_\theta(\theta - \theta_0)^2 + \sum_{dihedrals} \frac{V_n}{2}[1 + \cos(n\varphi - \gamma)] + \sum_{nonbonded} 4\varepsilon_{ij}\left(\left[\left(\frac{\sigma_{ij}}{r_{ij}}\right)^{12} - \left(\frac{\sigma_{ij}}{r_{ij}}\right)^{6}\right] + \left[\frac{q_i q_j}{\varepsilon R_{ij}}\right]\right) \quad (1)$$

The model for Compound **1** (Fig. 1) used for the QM calculations was built using GaussView [11]. All QM calculations were performed using Gaussian 03 [12]. The geometry was optimized using a two-step procedure, first at the HF/6-31G(d) and then at the B3LYP/6-31G(d) levels of theory. The restrained electrostatic potential (RESP) charge approach was used to derive atomic charges. First, the high-density ESP calculation was performed at B3LYP/6-31G(d) using the Merz-Kollman scheme. Then the charges were derived using Antechamber, which performed a two-stage charge fitting with default hyperbolic restraint parameters.

The other type of non-bonded parameters, the Van der Waals parameters, were taken from GAFF directly since they are known to be transferable as they are dependent mainly on the number of electrons in an atom rather than their chemical environment.

Two smaller systems derived from the optimized structure were used to calculate the missing parameters. An azido group attached to benzene, and an azido group attached to the methyl group of toluene were used as model systems for the aromatic and the aliphatic azido groups and are shown in Fig. 2. PES scans of the missing bonds, angles and dihedrals parameters were performed along the internal coordinates of the parameter of interest. All other parameters were kept fixed since the GAFF energy function that we want to fit does not contain cross-term potentials. The initial geometry optimization and subsequent single point energy calculations performed during the PES scans were carried out with B3LYP using the 6-311 +G(d) basis set. Bond scans were carried out using an increment of 0.002 Å for a total scan length of 0.04 Å centered on the equilibrium value. For bond angles, a 1° or 2° increment was used, with a total scan range varying from 15° to 30°.

Energy minimizations and MD simulations were performed using the Gromacs software package (version 3.3.3) [13–16]. Compound **1** was parameterized using GAFF [10, 17] as ported to Gromacs [18] and the newly developed parameters calculated for the $N_3$-Ar and $N_3$-Alk groups. TIP3P explicit solvent [19] was used to solvate the system. The simulations were run in a dodecahedral box containing 747 water molecules and using periodic boundaries conditions. The simulation box was created by placing the edge of the box at a minimum distance of 8 Å from the solute. The bonds in Compound **1** were constrained using the LINCS algorithm [20], while the bonds and the angles in the water molecules were constrained using the SETTLE algorithm [21]. A time step of 2 fs was used for integrating the equations of motion. The system was simulated in an NTP ensemble at a fixed temperature of 300 K and a fixed pressure of 1 bar. Temperature was kept constant using a Berendsen thermostat [22] with a coupling time of 0.1 ps, and pressure was controlled by a weak coupling to a reference pressure [22] with a coupling time of 1 ps and an

**Table 1** Geometric parameters calculated for the azido group of Probe **1**. *GAFF* Generalized Amber force field

| Bond[a] | Atom Type[b] | GAFF[c] R (Å)/$K_r$ | 6–31 G(d)[d] r (Å)/$K_r$ | 6–311 + G(d)[e] r (Å)/$K_r$ |
|---|---|---|---|---|
| C1–N1 ($N_3$–Ar) | ca-Ni | | | 1.421/380.9 |
| | ca-n2 | 1.470/320.6 | | |
| C7–N1 ($N_3$–Alk) | C3-Ni | | 1.490/277.5 | 1.491/293.5 |
| | C3-n2 | 1.477/313.8 | | |
| | C3-n3 | 1.470/320.6 | | |
| N1–N2 ($N_3$–Ar) | Ni-Nd | | | 1.231/758.3 |
| N1–N2 ($N_3$–Alk) | Ni-Nd | | 1.340/710.0 | 1.230/751.6 |
| | N2-n1 | 1.216/857.4 | | |
| | N3-n1 | 1.350/535.7 | | |
| | N2-n2 | 1.271/702.7 | | |
| N2–N3 ($N_3$–Ar) | Nd-Ne | | | 1.134/1329.4 |
| N2–N3 ($N_3$–Alk) | Nd-Ne | | 1.140/1312.0 | 1.135/1321.4 |
| | N1-n2 | 1.216/857.4 | | |
| | N1-n1 | 1.100/1365.7 | | |
| Angle[f] | | θ/$K_θ$ | θ/$K_θ$ | θ/$K_θ$ |
| C2–C1–N1 ($N_3$–Ar) | ca-ca-Ni | | | 119.95/163.4 |
| C1–C7–N1 ($N_3$–Alk) | ca-c3-Ni | | | 113.72/106.5 |
| | c3-c3-Ni | | 113.36/74.8 | |
| C1–N1–N2 ($N_3$–Ar) | ca-Ni-Nd | | | 118.73/81.4 |
| | ca-n2-n1 | NA | | |
| | ca-n2-n2 | 113.53/68.8 | | |
| C7–N1–N2 ($N_3$–Alk) | c3-Ni-Nd | | 115.60/64.0 | 115.81/68.4 |
| | c3-n2-n1 | 115.38/68.9 | | |
| | c3-n3-n1 | NA | | |
| | c3-n2-n2 | 111.18/69.3 | | |
| H7–C7–N1 ($N_3$–Alk) | h-c3-Ni | | 108.87/68.3 | 104.09/82.8 |
| N1–N2–N3 ($N_3$–Ar) | Ni-Nd-Ne | | | 172.83/43.0 |
| N1–N2–N3 ($N_3$–Alk) | Ni-Nd-Ne | | 173.54/42.4 | 173.40/42.6 |
| Torsion | | Vn[g]/2 | γ[h] | n[h] |
| $N_3$–Ar | | | | |
| c17–N3–N4–N5 | ca-Ni-Nd-Ne | 1.286 | 0 | 1 |
| c16–c17–N3–N4 | ca-ca-Ni-Nd | 3.477 | 180 | 2 |
| $N_3$–Alk | | | | |
| c21–N6–N7–N8 | c3-Ni-Nd-Ne | 1.167 | 0 | 1 |
| c19–c21–N6–N7 | ca-c3-Ni-Nd | 0.761 | 0 | 1 |
| c19–c21–N6–N7 | ca-c3-Ni-Nd | 0.269 | 0 | 3 |
| H22–c21–N6–N7 | h-c3-Ni-Nd | 0.761 | 0 | 1 |
| H22–c21–N6–N7 | h-c3-Ni-Nd | 0.269 | 0 | 3 |

[a] Bond length r (Å) and force constant $K_r$ (kcal mol$^{-1}$ Å$^{-2}$)

[b] Atom types follow GAFF nomenclature

[c] See [10]

[d] See [8]

[e] This work

[f] Angle θ value in (deg) and force constant $K_θ$ in (kcal mol$^{-1}$ deg$^{-2}$)

[g] Torsion potential (kcal mol$^{-1}$)

[h] Phase (deg) and multiplicity of the torsion angle

isothermal compressibility of 4.6 $10^{-5}$ bar$^{-1}$. Non-bonded interactions were calculated using a cut-off of 9 Å. Long-range Coulombic interactions were evaluated using particle mesh Ewald (PME) algorithm [23] with an interpolation order of 4 and Fourier spacing of 1.2 Å. The system was energy minimized and equilibrated for 200 ps after initial starting velocities were assigned randomly from a Maxwell distribution centered at 300 K. Finally, the production simulation was run for 20 ns.

## Results and discussion

The parameters resulting from the fitting of the QM PES are given in Table 1 and the statistical details of the calculations, such as the number of points in each data set, correlation coefficient *r* and F-values, are given in the electronic supplementary material. (Tables S1, S2) The F-value calculated for each model (bonds, angles and torsions) is much higher than its respective critical F-

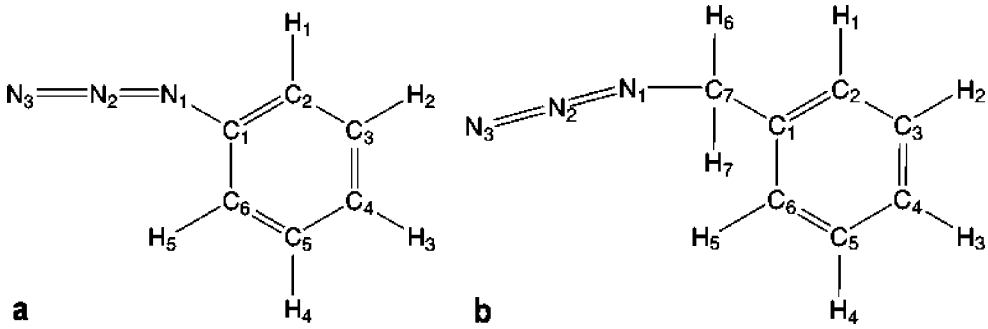


**Fig. 2** Schematic representations of the two subsystems used for the quantum mechanical (QM) potential energy surface (PES). **a** Subsystem containing the aromatic azido group. **b** Subsystem containing the aliphatic azido group

value at the 1% significance level. F-values range from 477 to 19,827 whereas the critical F-values are all below 12, indicating that all the models obtained from the fitting can be used to explain the data. The quality of the model, i.e., how well it correlates with the data, is given by the correlation coefficient *r*, which was higher than 0.990 for all the parameters (including dihedrals) with the exception of the torsion ca-c3-Ni-Nd for which *r* was equal to 0.983. These results indicate overall excellent correlation between the fitted MM force field potentials and the density functional theory (DFT)-based results.

Experimental studies on aliphatic azides [24–27] indicate that the N–N–N angle is close to 180°, suggesting that the middle nitrogen atom is best described as a mix between sp and, to a much lesser extent, $sp^2$ hybridization states. Because of this relatively unique electron distribution in the azido group none of the nitrogen atoms can be correctly described by the existing GAFF nitrogen atom types.

We started the development of the parameters by deciding whether the aryl and alkyl $N_3$ groups would require two different atom types for the nitrogen atom directly attached to the aromatic or aliphatic carbon atom. Interactions between the azide nitrogen atoms N1, N2 and N3, where N1, N2 and N3 correspond to the first, middle and last nitrogen atoms (Fig. 2a,b) of the azido groups, respectively, were examined using B3LYP and the 6-311 + G(d) basis set. The results obtained for the bonds N1–N2, N2–N3, and the angle N1–N2–N3 (Table 1) indicate that the force constants, the equilibrium bond length, and the angle values are almost identical for both the aliphatic and aromatic substituents with differences smaller than 1%. Thus, the same sets of atom types can be used for aromatic and aliphatic azido groups. For comparison with the previous parameterization publication we kept the same atom type names used in [8], where Ni, Nd and Ne correspond to N1, N2 and N3, respectively.

**Table 2** Atom types[a] and partial charges of the photoaffinity Probe **1**

| Name | Type | Charge | Name | Type | Charge | Name | Type | Charge |
|---|---|---|---|---|---|---|---|---|
| O1 | o | −0.5486 | H11 | hc | 0.1334 | C15 | ca | 0.0133 |
| N1 | n | −0.1639 | C7 | c | 0.6436 | C16 | ca | −0.2291 |
| H1 | hn | 0.2111 | O3 | o | −0.5398 | H19 | ha | 0.1361 |
| C1 | c | 0.481 | N2 | n | −0.4268 | C17 | ca | 0.3062 |
| O2 | o | −0.5811 | H12 | hn | 0.3004 | N3 | Ni | −0.4926 |
| C2 | c3 | −0.3478 | C8 | ca | 0.1818 | N4 | Nd | 0.6096 |
| H2 | hc | 0.0466 | C9 | ca | −0.2422 | N5 | Ne | −0.3878 |
| H3 | hc | 0.0466 | H13 | ha | 0.1377 | C18 | ca | −0.2824 |
| C3 | c3 | 0.097 | C10 | ca | −0.0941 | H20 | ha | 0.1557 |
| H4 | hc | −0.0053 | H14 | ha | 0.1332 | C19 | ca | −0.0087 |
| H5 | hc | −0.0053 | C11 | ca | −0.2634 | C21 | c3 | 0.1306 |
| C4 | c3 | −0.0408 | H15 | ha | 0.1378 | H21 | hc | 0.0661 |
| H6 | hc | 0.0197 | C12 | ca | 0.2999 | H22 | hc | 0.0661 |
| H7 | hc | 0.0197 | O4 | os | −0.3616 | C20 | ca | −0.1848 |
| C5 | c3 | 0.0545 | C13 | ca | −0.2328 | H23 | ha | 0.1334 |
| H8 | hc | 0.012 | H16 | ha | 0.1363 | N6 | Ni | −0.5464 |
| H9 | hc | 0.012 | C14 | c3 | 0.2274 | N7 | Nd | 0.6717 |
| C6 | c3 | −0.454 | H17 | hc | 0.0386 | N8 | Ne | −0.3917 |
| H10 | hc | 0.1334 | H18 | hc | 0.0386 | | | |

[a] Atom types follow GAFF nomenclature

With the azido group geometry and force characteristics independent of its substituent, the difference between the parameters covering the interface between the azido group and the substituent in $N_3$-Ar and $N_3$-Alk systems still required further evaluation. The differences observed in the bonds properties between ca-Ni (aromatic) and c3-Ni (aliphatic), in angle properties between ca-Ni-Nd and c3-Ni-Nd, ca-ca-Ni and ca-c3-Ni, and in dihedral properties indicate clearly that different parameters should be used to model $N_3$-Ar and $N_3$-Alk groups. This is notably the case for the bonds ca-Ni and c3-Ni, where the bond with the aromatic carbon is much shorter (1.421 Å) and stronger (380.9 kcal $mol^{-1}$ $Å^{-2}$) than its aliphatic equivalent (1.491 Å and 293.5 kcal $mol^{-1}$ $Å^{-2}$, respectively). The bond angles values for x–N1–N2 and x–x–N1 are similar in $N_3$-Ar and $N_3$-Alk groups, although, as expected, the force constants are greater for the parameters in the aromatic $N_3$-Ar group due to electron conjugation between its $N_3$ and aryl portions.

It should noted that, for the most part, the parameters for the aliphatic azido group are similar to those described in [8] with the main difference in the length of the bond Ni–Nd being shorter in our study (1.230 Å vs 1.340 Å). The bond length obtained in our calculations is in agreement with experimental values, reported to be 1.243 Å [24–26] for hydrazoic acid, 1.216 Å [24] and 1.240 Å [26] for azidomethane, and 1.229 Å [27] for azidoethane. When comparing these values with the equivalent parameters in GAFF, the N1–N2 bond characteristics appear as a combination of the characteristics of the bonds represented by GAFF atom types n2-n1, n3-n1 and n2-n2, where n3 corresponds to an $sp^3$ hybridized N atom, n2 to $sp^2$, and n1 to sp. This observation confirms that the middle nitrogen atom N2 is a mix of sp and $sp^2$ hybridization states.

Finally, since the main goal of this work was to obtain MM parameters to study dynamics of bis-azido Probe **1**, we also needed to determine the ligand atom charges. To calculate a reliable charge distribution in **1**, finding the correct protonation state of the hydroxamic acid is critical. With a $pK_a$ of 9.4, the hydroxamic acid is protonated in water at pH 7.4. However, there is evidence that this might not be the case for hydroxamate-based ligands when bound to the HDAC active site. It was shown that the $pK_a$ of hydroxamic acids decreases by ~3.3 log units upon forming a complex with the zinc atom in the HDAC catalytic site [28]. Therefore, the charges for the deprotonated state of Probe **1** were calculated. A schematic representation of Compound **1** were shown in Fig. 1 and the corresponding atom types and partial charges are given in Table 2.

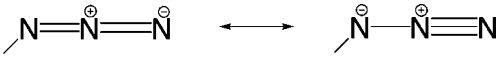

**Fig. 3** Resonance structures of the azido group

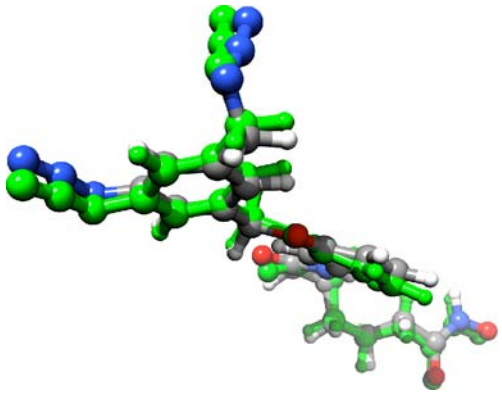

**Fig. 4** Comparison of the structures obtained after geometry optimization at the density functional theory (DFT) level (*gray*) and after energy minimization at the molecular mechanics (MM) level (*green*)

The high internal charges observed for the nitrogen atoms of the azido group are consistent with the main resonance structures of the azido group (Fig. 3), where the middle nitrogen carries a positive charge and either of the terminal nitrogen atoms carries a negative charge. The charges obtained for the deprotonated Probe **1** were found to be virtually identical to those obtained for azidobenzene and azidoethane, demonstrating that the charge distribution does not depend on the overall charge of the molecules but instead is specific to the azido group. The detailed results of these calculations are provided in the Tables S1 and S2.

To check the accuracy of the calculated parameters, we compared the structures obtained from the geometry optimization at the DFT level with the geometry obtained after energy minimization at the MM level using a tight convergence criterion of 1 kJ $mol^{-1}$ $nm^{-1}$ for the maximum force. The root mean square deviation (RMSD) between the heavy atoms of the two structures after least square fit was only 0.38 Å, indicating that the QM geometry could be reproduced accurately at the MM level. An overlay of Compound **1** optimized at the MM and QM levels is shown in Fig. 4.

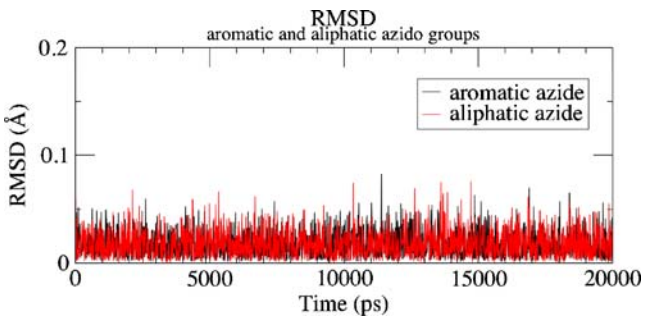


**Fig. 5** Root mean square deviation (RMSD) of the individual $N_3$-Ar and $N_3$-Alk azido groups during the course of the molecular dynamics (MD) simulation performed in water

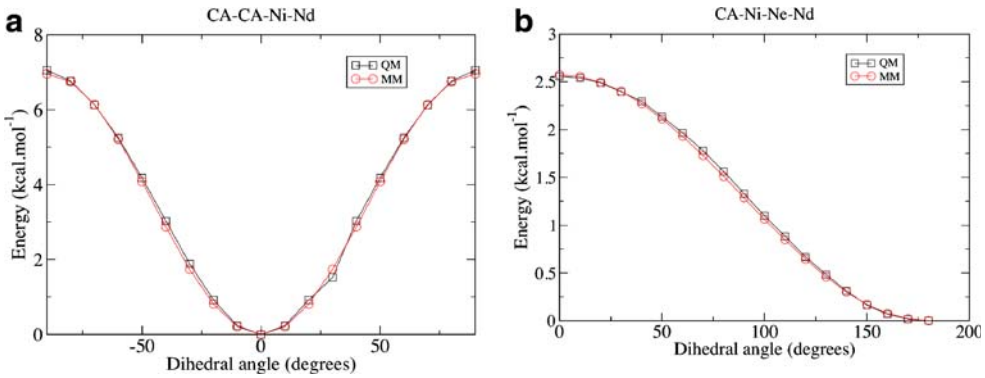


**Fig. 6** Comparison of the QM and MM rotational profiles calculated for the two dihedral angles of the aromatic azide. **a** Dihedral angle CA-CA-Ni-Nd, **b** dihedral angle CA-Ni-Nd-Ne

The parameters were further checked by performing MD simulations with the Gromacs software package of Ligand **1** in explicit solvent during a 20 ns production run. Figure 5 shows that the RMSD of each individual azide group is low throughout the course of the simulation, with fluctuation around 0.02 Å, indicating that bonds and angles remain close to their equilibrium values.

The dihedral potentials previously calculated for the model systems are shown in Fig. 6. Figure 7 shows that the distribution of the dihedral angles of the aromatic azido group is consistent with these previously calculated values. In the case of the dihedral CA-CA-Ni-Nd, the two minima observed at −90° and 90° in the dihedral distribution shown in Fig. 7a correspond to the maxima of the dihedral potential shown in Fig. 6a. Similarly, the two maxima at 0° and 180° in the dihedral distribution match the minima in the dihedral potential. In the case of the dihedral CA-Ni-Nd-Ne, there is only one maximum at 180° and one minimum at 0° in the dihedral distribution (Fig. 7b), and both are consistent with the minimum and maximum observed in the dihedral potential (Fig. 6b). The dihedral distribution for the dihedral CA-CA-Ni-Nd-Ne shows that the most dominant conformations of the aromatic azido group correspond to a coplanar arrangement with the aromatic ring. This effect is expected to be due to π electron delocalization between the π orbitals of the phenyl ring and of the azide group, and is represented in the MM model by the potential well. There is a strong energy penalty for leaving the planar arrangement; however, the potential still allows interconversion at 300 K between the two dihedral minima since they both appear equally populated.

Overall, the results suggest that the parameters are well suited for reproducing the geometry of the azido groups during energy minimizations. An analysis of the MD data for Ligand **1** shows that the potential energy and its components oscillate around their average values and remain stable during the extensive MD simulation in water, suggesting that the parameters are suitable for MD simulation studies.

## Conclusions

GAFF parameters for $N_3$-Ar and $N_3$-Alk were calculated. The quality of the parameters was confirmed by accurately reproducing the QM PES. Our study indicates that the three new nitrogen atom types are likely to be sufficient to describe both the $N_3$-Ar and $N_3$-Alk groups in small organic molecules in MM force fields. Further analysis has shown that two different sets of bond, angle, and torsion parameters for the group of atoms consisting of the nitrogen atoms in the azido group and the adjacent carbon atoms should be used to describe these systems. As expected, the force constants for the bonds and angles of the $N_3$-Ar azido group are greater than those for $N_3$-Alk

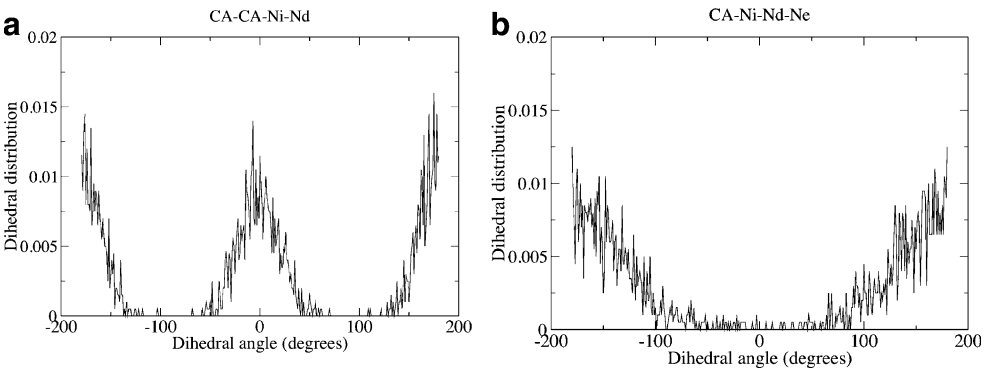


**Fig. 7** Distribution of the dihedral angles obtained during MD simulation. **a** Dihedral CA-CA-Ni-Nd, **b** dihedral CA-Ni-Nd-Ne

group because of the effect of delocalization in the former group. The parameters were tested in an MD simulation of the hydroxamate HDAC Probe **1** in water. The system was found to be stable, indicating that the parameters are suitable for MD simulations of, and should be useful for, computational studies of ligands containing either or both $N_3$-Ar and $N_3$-Alk groups.

**Acknowledgments** We would like to thank Dr. Michael Brünsteiner for critical analysis of the manuscript. This study was funded in part by the Breast Cancer Congressionally Directed Research Program of Department of Defense Idea Award BC051554 and by the National Cancer Institute/NIH grant 1R01 CA131970-01A1. We also thank OpenEye Scientific Software for providing academic license for modeling software.

## References

1. He B et al (2009) Photolabeling probes for mapping the multiple binding poses of HDAC inhibitors. In: Abstract of papers of AACR-ACS Chemistry in Cancer Research: A Vital Partnership in Cancer Drug Discovery and Development. New Orleans, LA, p A5
2. Kouzarides T (1999) Histone acetylases and deacetylases in cell proliferation. Curr Opin Genet Dev 9:40–48
3. Archer SY, Hodin RA (1999) Histone acetylation and cancer. Curr Opin Genet Dev 9:171–174
4. Cress WD, Seto E (2000) Histone deacetylases, transcriptional control, and cancer. J Cell Physiol 184:1–16
5. Mahlknecht U, Ottmann OG, Hoelzer D (2000) When the band begins to play: histone acetylation caught in the crossfire of gene control. Mol Carcinog 27:268–271
6. Hahnen E et al (2008) Histone deacetylase inhibitors: possible implications for neurodegenerative disorders. Expert Opin Investig Drugs 17:169–184
7. Kozikowski AP et al (2007) Functional differences in epigenetic modulators—superiority of mercaptoacetamide-based histone deacetylase inhibitors relative to hydroxamates in cortical neuron neuroprotection studies. J Med Chem 50:3054–3061
8. Carvalho ATP, Fernandes PA, Ramos MJ (2007) Parameterization of AZT—a widely used nucleoside inhibitor of HIV-1 reverse transcriptase. Int J Quantum Chem 107:292–298
9. Cornell WD et al (1995) A second generation force field for the simulation of proteins, nucleic acids, and organic molecules. J Am Chem Soc 117:5179–5197
10. Wang J et al (2004) Development and testing of a general amber force field. J Comput Chem 25:1157–1174
11. Dennington R II et al (2003) GaussView. Semichem Inc, Shawnee Mission, KS
12. Frisch MJ et al (2004) Gaussian 03, Revision C.02. Gaussian Inc, Wallingford, CT
13. Berendsen HJC, Spoel Dvd, Drunen Rv (1995) GROMACS: a message-passing parallel molecular dynamics implementation. Comp Phys Commun 91:43–56
14. Lindal E, Hess B, Spoel Dvd (2001) GROMACS 3.0: a package for molecular simulation and trajectory analysis. J Mol Model 7:306–317
15. van der Spoel D et al (2001) Gromacs User Manual Version 3.0. Nijenborgh, Groningen, Netherlands. Internet: http://www.gromacs.org
16. van der Spoel D et al (2005) Gromacs: fast, flexible and free. J Comput Chem 26:1701–1718
17. Wang J et al (2006) Automatic atom type and bond type perception in molecular mechanical calculations. J Mol Graphics Modell 25:247–260
18. Sorin EJ, Rhee YM, Pande VS (2005) Does water play a structural role in the folding of small nucleic acids? Biophys J 88:2516–2524
19. Jorgensen WL et al (1983) Comparison of simple potential functions for simulating liquid water. J Chem Phys 79:926–935
20. Hess B et al (1997) LINCS: a linear constraint solver for molecular simulations. J Comput Chem 18:1463–1472
21. Miyamoto S, Kollman PA (1992) SETTLE: an analytical version of the SHAKE and RATTLE algorithms for rigid water models. J Comput Chem 13:952–962
22. Berendsen HJC et al (1984) Molecular dynamics with coupling to an external bath. J Chem Phys 81:3684–3690
23. Darden T, York D, Pedersen L (1993) Particle mesh Ewald: An N-log(N) method for Ewald sums in large systems. J Chem Phys 98:10089–10092
24. Anderson DWW, Rankin DWH, Robertson A (1972) Electron diffraction determination of the molecular structures of methyl-azide, methylisocyanate and methylisothiocyanate in the gas phase. J Mol Structure 14:385–396
25. Winnewisser BP (1980) The substitution structure of hydrazoic acid, HNNN. J Mol Spectrosc 82:220–223
26. Klaeboe P et al (1986) The vibrational spectra, molecular structure and conformation of organic azides. Part I. A survey. J Mol Struct 141:161–172
27. McQuaid MJ, Sun H, Rigby D (2004) Development and validation of COMPASS force field parameters for molecules with aliphatic azide chains. J Comput Chem 25:61–71
28. Cross JB et al (2002) The active site of a zinc-dependent metalloproteinase influences the computed pK(a) of ligands coordinated to the catalytic zinc ion. J Am Chem Soc 124:11004–11007